JCTC Journal of Chemical Theory and Computation

pubs.acs.org/JCTC Article

Linear-Response Time-Dependent Density Functional Theory with Stochastic Range-Separated Hybrids

Xu Zhang,* Gang Lu, Roi Baer, Eran Rabani, and Daniel Neuhauser*

Cite This: J. Chem. Theory Comput. 2020, 16, 1064−1072 Read Online

ACCESS | Metrics & More | Article Recommendations

ABSTRACT: Generalized Kohn−Sham density functional theory is a popular computational tool for the ground state of extended systems, particularly within range-separated hybrid (RSH) functionals that capture the long-range electronic interaction. Unfortunately, the heavy computational cost of the nonlocal exchange operator in RSH-DFT usually confines the approach to systems with at most a few hundred electrons. A significant reduction in the computational cost is achieved by representing the density matrix with stochastic orbitals and a stochastic decomposition of the Coulomb convolution (*J. Phys. Chem. A* **2016,** *120,* 3071). Here, we extend the stochastic RSH approach to excited states within the framework of linear-response generalized Kohn−Sham time-dependent density functional theory (GKS-TDDFT) based on the plane-wave basis. As a validation of the stochastic GKS-TDDFT method, the excitation energies of small molecules N_2 and CO are calculated and compared to the deterministic results. The computational efficiency of the stochastic method is demonstrated with a two-dimensional MoS_2 sheet (∼1500 electrons), whose excitation energy, exciton charge density, and (excited state) geometric relaxation are determined in the absence and presence of a point defect.

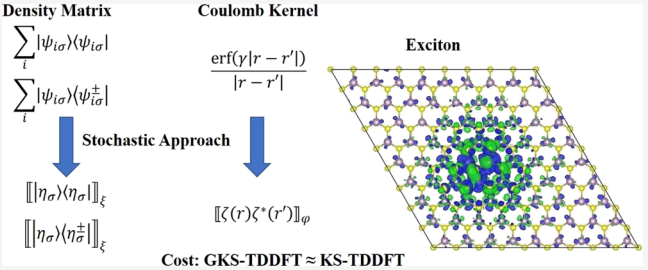

I. INTRODUCTION

Understanding, predicting, and ultimately controlling excited-state behavior are central to diverse chemical, molecular, and material problems, including photovoltaics, light-emitting devices, photocatalysis, photosynthesis, plasmonics, molecular electronics, and biosensors. Nowadays, time-dependent density functional theory (TDDFT)[1,2] has become one of the most powerful tools to probe the electronic structure and optical excitations, balancing computational accuracy and efficiency. In particular, linear-response TDDFT has been widely employed to compute the excitation energy, ionic force, and nonadiabatic coupling of excited states in molecular- and solid-state materials.[3−15]

Exchange−correlation (XC) functionals play a critical role in both DFT and TDDFT. It is well-known that semi-local XC functionals, such as the generalized-gradient approximation (GGA) and the local density approximation, do not accurately predict excited-state properties in ***extended*** systems because of the incorrect description of long-range electron−electron and electron−hole interaction.[16−18] In contrast, generalized Kohn−Sham (GKS)[19,20] DFT and TDDFT methods with a nonlocal exchange interaction (hybrid functionals)[21,22] have been shown to yield accurate one- and two-particle excitations, for both molecular and extended systems.[23−29] Note that here, GKS refers specifically to the inclusion of explicit exchange but not to the use of mixed-spin orbitals.

The majority of existing GKS-TDDFT codes uses atom-centered (AO) basis sets with target applications in molecular chemistry.[30−32] The most important advantage of AO bases is that hybrid functionals are readily computed with short-range AOs; the scaling of operating with a nonlocal exchange is $O(N^2)$ in a local basis (but with a possibly large prefactor, depending on the AO basis and its degree of localization). In contrast, a plane-wave basis is a natural choice for periodic and extended systems, thanks to its simplicity and completeness. In addition, it is free of Pulay forces that plague AO basis methods. The drawback of plane waves is that hybrid functionals are computationally demanding because the nonlocal exchange is obtained from the density matrix rather than the density, increasing the scaling from $O(N^2 \log N)$ in KS-TDDFT to $O(N^3 \log N)$ in GKS-TDDFT.

To alleviate the cost of hybrid functionals, one can unitarily transform all occupied orbitals into spatially localized ones.[33−35] The nonlocal exchange potential and the corresponding exchange energy are then calculated efficiently with the localized orbitals.[36−38] Recently, Lin has introduced an adaptively compressed exchange operator with a low rank that

Received: November 11, 2019
Published: January 3, 2020

Downloaded via UNIV OF CALIFORNIA LOS ANGELES on November 12, 2020 at 10:53:08 (UTC).
See https://pubs.acs.org/sharingguidelines for options on how to legitimately share published articles.

© 2020 American Chemical Society

https://dx.doi.org/10.1021/acs.jctc.9b01121
J. Chem. Theory Comput. 2020, 16, 1064−1072

significantly reduces the computational cost of nonlocal exchange.[39] These methods work well in GKS-DFT, as it involves only the occupied orbitals.

Here, we extend the recently developed stochastic orbital method to efficiently describe excited states in plane-wave based linear-response GKS-TDDFT, by significantly reducing the cost of the exchange operator. With the stochastic approach, the numerically expensive explicit-exchange GKS Hamiltonian becomes, for large systems, as cheap as a local-potential KS Hamiltonian.[40] Recently, a real time GKS-TDDFT with a stochastic hybrid functional (the same functional used here) was developed and applied to calculate absorption spectra for large finite phosphorene sheets containing up to 2000 electrons.[41] Furthermore, stochastic KS-DFT,[42] stochastic GW,[43] and stochastic Bethe−Salpeter equation (BSE)[44] were successfully applied to systems with thousands of electrons.

The present work merges the efficiency of the stochastic approach in describing hybrid functionals with the efficiency of frequency-based TDDFT in describing low-frequency excitations. Specifically, we reformulate plane-wave based linear-response GKS-TDDFT by using a stochastic representation of hybrid functionals. We concentrate on long-range-separated hybrid (RSH) functionals with an optimally tuned range-separation parameter.[45−49] In Section II, we first present GKS-TDDFT with a deterministic RSH functional. The stochastic formulation of the RSH functional is introduced. Then, we briefly analyze the cost saving with stochastic GKS-TDDFT. Lastly, we present the implementation of the projector augmented-wave (PAW) pseudopotential[50,51] and the required modification of the stochastic exchange formula. In Section III, the method is validated for two small molecules, N_2 and CO, and is then applied to a two-dimensional (2D) MoS_2 sheet with almost 1500 electrons. Finally, we conclude in Section IV.

II. METHODOLOGY

We only consider the Γ-point in the Brillouin zone, where we use real KS orbitals. In the following, we use the indices i, j, k ... to label occupied KS orbitals; σ, τ ... to denote their spins; and α, β ... to label excited states.

A. TDDFT Formalism Using Deterministic RSHs. The action of the GKS Hamiltonian on each KS orbital is

$$H^\sigma|\psi_{i\sigma}\rangle = \left(-\frac{1}{2}\nabla^2 + V_{\mathrm{loc}}^\sigma + V_{\mathrm{NL}} + k_\sigma^\gamma\right)|\psi_{i\sigma}\rangle \tag{1}$$

where V_{loc}^σ is the KS effective local potential, consisting of Hartree, local XC, and local pseudopotential terms. V_{NL} is the nonlocal pseudopotential. k_σ^γ is the range-separated exchange operator that acts on the KS orbital as

$$k_\sigma^\gamma|\psi_{i\sigma}\rangle = -\sum_j \int \psi_{j\sigma}(r)u_{\mathrm{C}}^\gamma(|r-r'|)\psi_{j\sigma}^*(r')\psi_{i\sigma}(r')\mathrm{d}r' \tag{2}$$

Here, $u_{\mathrm{C}}^\gamma(r) = r^{-1}\,\mathrm{erf}(\gamma r)$ accounts for long-range contributions to the nonlocal exchange and γ is the range-separation parameter. The ground-state GKS-DFT equation is then

$$H^\sigma|\psi_{i\sigma}\rangle = \sum_j \epsilon_{ij\sigma}|\psi_{j\sigma}\rangle \tag{3}$$

with the orthonormal condition $\langle\psi_{i\sigma}|\psi_{j\tau}\rangle = \delta_{ij}\delta_{\sigma\tau}$ and $\epsilon_{ij\sigma} = \delta_{ij}\epsilon_{i\sigma}$ is the energy of the ith KS orbital.

The excited-state energies and wave functions can be obtained by solving a non-Hermitian eigenvalue equation

$$\begin{pmatrix}\mathbf{A} & \mathbf{B}\\ \mathbf{B} & \mathbf{A}\end{pmatrix}\begin{pmatrix}\boldsymbol{\psi}_\alpha^+\\ \boldsymbol{\psi}_\alpha^-\end{pmatrix} = \omega_\alpha\begin{pmatrix}-\mathbf{I} & 0\\ 0 & \mathbf{I}\end{pmatrix}\begin{pmatrix}\boldsymbol{\psi}_\alpha^+\\ \boldsymbol{\psi}_\alpha^-\end{pmatrix} \tag{4}$$

which is analogous to Casida's equation.[3] Here, ω_α is the αth excitation energy, $\mathbf{I}$ is the identity matrix, and $\boldsymbol{\psi}_\alpha^\pm$ is the linear-response orbital. Note that the linear-response orbital $|\psi_{i\sigma}^+\rangle$ corresponds to $\sum_b X_{ib\sigma}|\psi_{b\sigma}\rangle$ in Casida's equation and $|\psi_{i\sigma}^-\rangle$ corresponds to $\sum_b Y_{ib\sigma}|\psi_{b\sigma}\rangle$, where b labels the unoccupied KS orbitals. $\sum_i(|\psi_{i\sigma}\rangle\langle\psi_{i\sigma}^+| + |\psi_{i\sigma}^-\rangle\langle\psi_{i\sigma}|)$ represents the KS transition density matrix. The linear-response orbital is directly expanded by the plane-wave basis in the virtual space which is orthogonal to the occupied orbitals. The use of the plane-wave representation with a projector to remove the contribution of the occupied space avoids the need to obtain all the (unknown) virtual orbitals and enables the efficient calculations of absorption spectra.[52,53]

The matrix operators $\mathbf{A}$ and $\mathbf{B}$ act on the linear-response orbitals

$$\begin{aligned}[\mathbf{A}\boldsymbol{\psi}^\pm]_{i\sigma} &= \sum_j (H^\sigma\delta_{ij} - \epsilon_{ij\sigma})|\psi_{j\sigma}^\pm\rangle \\ &\quad + \sum_{j\tau}\langle P_c^\sigma\psi_{i\sigma}|K_{\sigma\tau}|\psi_{j\tau}P_c^\tau\psi_{j\tau}^\pm\rangle\\ [\mathbf{B}\boldsymbol{\psi}^\pm]_{i\sigma} &= \sum_{j\tau}\langle P_c^\sigma\psi_{i\sigma}|K_{\sigma\tau}|P_c^\tau\psi_{j\tau}^\pm\psi_{j\tau}\rangle\end{aligned} \tag{5}$$

where $P_c^\sigma = 1 - \sum_i|\psi_{i\sigma}\rangle\langle\psi_{i\sigma}|$ is a projection operator to the virtual space which is required to avoid the explicit use of virtual orbitals and $K_{\sigma\tau}$ is the Hartree and XC kernel. The kernel is labeled as (note that the expression below is a function of r)

$$\begin{aligned}\langle\psi_{j\sigma}|K_{\sigma\tau}|\psi_{k\tau}\psi_{l\tau}\rangle &= \int\psi_{j\sigma}(r)\left(\frac{1}{|r-r'|} + \frac{\delta^2E_{\mathrm{xc}}}{\delta n^\sigma(r)\delta n^\tau(r')}\right)\\ &\quad \psi_{k\tau}^*(r')\psi_{l\tau}(r')\mathrm{d}r'\\ &\quad - \delta_{\sigma\tau}\int\psi_{l\sigma}(r)u_{\mathrm{C}}^\gamma(|r-r'|)\\ &\quad \psi_{k\sigma}^*(r')\psi_{j\sigma}(r')\mathrm{d}r'\end{aligned} \tag{6}$$

Here, $n^\sigma(r)$ is the charge density with spin σ and E_{xc} is the local XC functional. The last term in eq 6 is the RSH element, denoted henceforth as $\langle\psi_{j\sigma}|K_{\mathrm{RSH}}|\psi_{k\tau}\psi_{l\tau}\rangle$. We employ an iterative algorithm[54] to determine the low-lying eigenvalues and eigenvectors of the large non-Hermitian matrix in eq 4.

A Lagrangian is constructed to calculate the ionic force associated with the αth excited state[11]

$$\begin{aligned}\hat{\mathcal{L}}_\alpha[x,\psi,\mathbf{Z},\mathbf{\Gamma}] &= \mathcal{M}[x,\psi] + \sum_{ij\sigma}\langle Z_{i\sigma}|(H^\sigma\delta_{ij} - \varepsilon_{ij\sigma})|\psi_{j\sigma}\rangle\\ &\quad - \sum_{i\geq j,\sigma}\Gamma_{ij\sigma}(\langle\psi_{i\sigma}|\psi_{j\sigma}\rangle - \delta_{ij})\end{aligned} \tag{7}$$

by enforcing the Brillouin condition and the orthonormal condition for the KS orbitals, where x denotes the ionic coordinate. In the abovementioned equation, the functional $\mathcal{M}$ is

$$\mathcal{M} \equiv (\boldsymbol{\psi}_\alpha^+\ \ \boldsymbol{\psi}_\alpha^-)\left[\begin{pmatrix}\mathbf{A} & \mathbf{B}\\ \mathbf{B} & \mathbf{A}\end{pmatrix} + \omega_\beta\begin{pmatrix}\mathbf{I} & 0\\ 0 & -\mathbf{I}\end{pmatrix}\right]\begin{pmatrix}\boldsymbol{\psi}_\alpha^+\\ \boldsymbol{\psi}_\alpha^-\end{pmatrix} \tag{8}$$

https://dx.doi.org/10.1021/acs.jctc.9b01121
J. Chem. Theory Comput. 2020, 16, 1064−1072

The multipliers $\mathbf{Z}$ and $\mathbf{\Gamma}$ are determined from the stationary condition of the Lagrangian $\delta\hat{\mathcal{L}}_\alpha/\delta\psi_i = 0$. The ionic force in the excited states is the partial derivative of the Lagrangian with respect to the ionic coordinate $F_\alpha = -\partial\hat{\mathcal{L}}_\alpha/\partial x$, while the charge density of the αth excited state is obtained from the derivative of the Lagrangian with respect to the external potential, $\rho_\alpha^{\mathrm{ex}} = -\delta\hat{\mathcal{L}}_\alpha/\delta V_{\mathrm{ext}}$.

B. Stochastic Representation of RSHs in TDDFT. Following ref 40, we introduce an occupied-projected random orbital

$$|\eta_\sigma\rangle = \sum_i |\psi_{i\sigma}\rangle\langle\psi_{i\sigma}|\xi\rangle \tag{9}$$

Here, $\xi(r) = \pm 1/\sqrt{\Delta V}$ are random functions, with a random sign at each real-space grid point, and ΔV is the volume per grid point. A stochastic representation of the identity operator is expressed as[55]

$$[|\xi\rangle\langle\xi|]_\xi = 1 \tag{10}$$

where $[\cdots]_\xi$ denotes the average over all random functions ξ. Thus, we use the stochastic orbitals to calculate the zero-order KS density matrix

$$[|\eta_\sigma\rangle\langle\eta_\sigma|]_\xi = \sum_{ij} [|\psi_{i\sigma}\rangle\langle\psi_{i\sigma}|\xi\rangle\langle\xi|\psi_{j\sigma}\rangle\langle\psi_{j\sigma}|]_\xi = \sum_i |\psi_{i\sigma}\rangle\langle\psi_{i\sigma}| \tag{11}$$

The range-separated exchange kernel is also determined stochastically

$$u_C^\gamma(|r - r'|) = [\zeta(r)\zeta^*(r')]_\varphi \tag{12}$$

with

$$\zeta(r) = \frac{1}{(2\pi)^3}\int \sqrt{\bar{u}_C^\gamma(k)}\ e^{i\varphi(k)}\ e^{ik\cdot r}\ dk \tag{13}$$

where $\bar{u}_C^\gamma(k)$ is the Fourier transform of $u_C^\gamma(r)$ and $\varphi(k)$ is a random phase (with a value between 0 and 2π) at each k point.

By defining a stochastic orbital $|\chi_\sigma\rangle$,

$$|\chi_\sigma\rangle = \zeta(r)|\eta_\sigma\rangle \tag{14}$$

we then have the stochastic formulation of the RSH in the GKS Hamiltonian as

$$k_\sigma^\gamma|\psi_{i\sigma}\rangle = -[|\chi_\sigma\rangle\langle\chi_\sigma|\psi_{i\sigma}\rangle]_{\xi,\varphi} \tag{15}$$

In actual applications, we construct and store in memory a priori a finite number N_χ of pairs of random functions $\{\xi(r),\zeta(k)\}$. The stochastic orbitals $|\chi_\sigma\rangle$ are calculated on the fly with the updated KS-occupied orbitals $|\psi_{i\sigma}\rangle$.

Next, we present the stochastic formulation of RSHs in the context of eq 5. The occupied-projected random linear-response orbital is introduced as

$$|\eta_\sigma^\pm\rangle = \sum_i |\psi_{i\sigma}^\pm\rangle\langle\psi_{i\sigma}|\xi\rangle \tag{16}$$

which leads to a stochastic representation of the first-order KS density matrix as

$$\sum_i (|\psi_{i\sigma}\rangle\langle\psi_{i\sigma}^\pm| + |\psi_{i\sigma}^\pm\rangle\langle\psi_{i\sigma}|) = [|\eta_\sigma\rangle\langle\eta_\sigma^\pm| + |\eta_\sigma^\pm\rangle\langle\eta_\sigma|]_\xi \tag{17}$$

The stochastic linear-response orbital $|\chi_\sigma^\pm\rangle$ is then defined as

$$|\chi_\sigma^\pm\rangle = \zeta(r)|\eta_\sigma^\pm\rangle \tag{18}$$

The RSH components in eq 5 can thus be calculated stochastically because

$$\sum_j \langle\psi_{i\sigma}|K_{\mathrm{RSH}}|\psi_{j\sigma}\psi_{j\sigma}^\pm\rangle = -[|\chi_\sigma^\pm\rangle\langle\chi_\sigma|\psi_{i\sigma}\rangle]_{\xi,\varphi} \tag{19}$$

and

$$\sum_j \langle\psi_{i\sigma}|K_{\mathrm{RSH}}|\psi_{j\sigma}^\pm\psi_{j\sigma}\rangle = -[|\chi_\sigma\rangle\langle\chi_\sigma^\pm|\psi_{i\sigma}\rangle]_{\xi,\varphi} \tag{20}$$

In linear-response TDDFT, all occupied orbitals $|\psi_{i\sigma}\rangle$ are fixed and the stochastic linear-response orbitals $|\chi_\sigma^\pm\rangle$ are calculated on the fly by using the updated linear-response orbitals $|\psi_{i\sigma}^\pm\rangle$.

C. Cost Saving with Stochastic TDDFT. The numerically dominant cost is the action of the exchange. We now briefly analyze the savings because of the use of stochastic exchange, following ref 40. In deterministic GKS-DFT and GKS-TDDFT, when acting with the exchange kernel on all occupied orbitals, there are $N_{\mathrm{occ}}{}^2$ (i.e., all pairs) Coulomb convolution integrals, each costing about $10N_{\mathrm{plw}}\log_2 N_{\mathrm{plw}}$ double-precision operations. The number of operations is about $200N_{\mathrm{plw}}$ for large system sizes with $N_{\mathrm{plw}} \approx 10^5$–$10^7$. Thus, the total cost per action of the exchange is about $200N_{\mathrm{occ}}{}^2N_{\mathrm{plw}}$. In contrast, in the stochastic exchange [eqs 15, 19, and 20], the cost per occupied orbital is twice that of applying N_χ dot products, each costing $2N_{\mathrm{plw}}$, that is, the total exchange-kernel cost per iteration is circa $4N_\chi N_{\mathrm{occ}}N_{\mathrm{plw}}$. Therefore, the ratio of the cost between deterministic and stochastic exchange is 50 N_{occ}/N_χ.

For small systems, where a large range-separation parameter γ is used, N_χ is around 1000, so the breakeven point is around 20 occupied orbitals, that is, systems with few tens of electrons. For large systems with thousands of electrons, $N_\chi \approx 50$–100 is sufficient to yield converged results. Thus, the stochastic calculation saves about a factor of around N_{occ} relative to the deterministic calculation. For such large systems, the cost of applying the stochastic exchange is no more than that of local-exchange (or no-exchange) KS-TDDFT, where the computationally most demanding step is applying the kinetic energy (circa $200N_{\mathrm{occ}}N_{\mathrm{plw}}$). Thus, the stochastic exchange GKS-TDDFT for large systems just approximately doubles the cost of no-exchange KS-TDDFT (i.e., linear-response random-phase approximation).

These considerations do not change when we use PAW, as detailed in the next section. Also, note that the underlying TDDFT approach is based on the plane-wave basis so that it is fully converged with respect to the virtual orbital basis. It is possible to also employ similar stochastic-TDDFT approaches with any AO basis sets, highly local or not, although this will not be pursued here.

D. PAW Formalism. Pseudopotentials are routinely used in conjunction with plane-wave methods. Here, we focus on the PAW pseudopotential, which provides a higher transferability and a lower energy cutoff than the norm-conserving pseudopotentials.[56,57] In PAW, the all-electron (AE) wave function $|\psi_{i\sigma}\rangle$ is a linear transformation of the pseudo-wave-function (PS) $|\tilde{\psi}_i$

$$|\psi_{i\sigma}\rangle = \mathcal{T}|\tilde{\psi}_{i\sigma}\rangle = |\tilde{\psi}_{i\sigma}\rangle + \sum_I (|\phi_I\rangle - |\tilde{\phi}_I\rangle)\langle\tilde{p}_I|\tilde{\psi}_{i\sigma}\rangle \tag{21}$$

where ϕ_I, $\tilde{\phi}_I$, and $\tilde{p}_I$ are AE partial waves, PS partial waves, and projector functions, respectively, defined in the core region.

https://dx.doi.org/10.1021/acs.jctc.9b01121
J. Chem. Theory Comput. 2020, 16, 1064−1072

The index I also includes the angular momentum quantum numbers and an additional index for the reference energy. In the following, the tilde symbols represent the PS wave functions and operators, which are evaluated on the plane-wave grid. By using PAW, the ground-state GKS equation in eq 3 is expressed as

$$\tilde{H}^{\sigma}|\tilde{\psi}_{i\sigma}\rangle = \sum_{j} \epsilon_{ij\sigma}\tilde{S}|\tilde{\psi}_{j\sigma}\rangle \tag{22}$$

with the orthonormal condition $\langle\tilde{\psi}_{i\sigma}|\tilde{S}|\tilde{\psi}_{j\tau}\rangle = \delta_{ij}\delta_{\sigma\tau}$ and $\tilde{S} = \mathcal{T}^{\dagger}\mathcal{T}$ is the overlap operator.

The action of the GKS Hamiltonian on the PS orbital is given by[51,58]

$$\begin{aligned}\tilde{H}^{\sigma}|\tilde{\psi}_{i\sigma}\rangle = &\left(-\frac{1}{2}\nabla^2 + \tilde{V}^{\sigma}_{\mathrm{loc}}\right)|\tilde{\psi}_{i\sigma}\rangle \\ &+ \sum_{IJ}|\tilde{p}_I\rangle(\hat{D}_{IJ}[\tilde{V}^{\sigma}_{\mathrm{loc}}] + D^1_{IJ} - \tilde{D}^1_{IJ})\langle\tilde{p}_J|\tilde{\psi}_{i\sigma}\rangle \\ &+ \tilde{k}^{\gamma}_{\sigma}|\tilde{\psi}_{i\sigma}\rangle\end{aligned} \tag{23}$$

Here, we have several additional PAW terms compared to eq 1. The PAW tensor in the Hamiltonian is $\hat{D}_{IJ}[\tilde{V}] = \sum_{LM}\int\tilde{V}(r)\hat{Q}^{LM}_{IJ}(r)\mathrm{d}r$ and for the definitions of the functions $\hat{Q}^{LM}_{IJ}(r)$, see, for example, Eq 27 of ref 51. The difference $(D^1_{IJ} - \tilde{D}^1_{IJ})$ is calculated as $\partial(E^1 - \tilde{E}^1)/\partial\rho^{\sigma}_{IJ}$, where E^1 and $\tilde{E}^1$ are parts of the total energy computed on the radial grid[51] and $\rho^{\sigma}_{IJ} = \sum_i\langle\tilde{\psi}_{i\sigma}|\tilde{p}_I\rangle\langle\tilde{p}_J|\tilde{\psi}_{i\sigma}\rangle$ is the occupancy of each augmentation channel (I, J).

Within PAW, the range-separated exchange operator $\tilde{k}^{\gamma}_{\sigma}$ acts on the PS orbital as

$$\begin{aligned}\tilde{k}^{\gamma}_{\sigma}|\tilde{\psi}_{i\sigma}\rangle = &-\sum_{j}\tilde{V}_{\mathrm{RSH}}[\tilde{n}_{ji\sigma} + \hat{n}_{ji\sigma}]|\tilde{\psi}_{j\sigma}\rangle \\ &- \sum_{j,IJ}|\tilde{p}_I\rangle\hat{D}_{IJ}[\tilde{V}_{\mathrm{RSH}}]\langle\tilde{p}_J|\tilde{\psi}_{j\sigma}\rangle \\ &- \sum_{(I,K)(J,L)}(K^1_{IJLK} - \tilde{K}^1_{IJLK})\rho^{\sigma}_{LJ}|\tilde{p}_I\rangle\langle\tilde{p}_K|\tilde{\psi}_{i\sigma}\rangle\end{aligned} \tag{24}$$

Here, $\tilde{V}_{\mathrm{RSH}}$ is the range-separated exchange potential, expressed as

$$\tilde{V}_{\mathrm{RSH}}[\tilde{n}_{ji\sigma} + \hat{n}_{ji\sigma}] = \int u^{\gamma}_{\mathrm{C}}(|r - r'|)[\tilde{n}_{ji\sigma}(r') + \hat{n}_{ji\sigma}(r')]\mathrm{d}r' \tag{25}$$

where $\tilde{n}_{ij\sigma} = \tilde{\psi}^{*}_{i\sigma}\tilde{\psi}_{j\sigma}$ is the PS charge density and $\hat{n}$ is the compensation charge density

$$\hat{n}_{ij\sigma}(r) = \sum_{IJ,LM}\langle\tilde{\psi}_{i\sigma}|\tilde{p}_I\rangle\langle\tilde{p}_J|\tilde{\psi}_{j\sigma}\rangle\hat{Q}^{LM}_{IJ}(r) \tag{26}$$

Both $\tilde{n}$ and $\hat{n}$ are calculated on the uniform plane-wave grid. K^1_{IJLK} $(\tilde{K}^1_{IJLK})$ is the two-electron four-AE (PS)-partial-wave integral[58] obtained using the range-separated exchange kernel $u^{\gamma}_{\mathrm{C}}(r)$.

By using PAW, the kernel in eq 6 becomes[15]

$$\begin{aligned}\langle\tilde{\psi}_{j\sigma}|\tilde{K}_{\sigma\tau}|\tilde{\psi}_{k\tau}\tilde{\psi}_{l\tau}\rangle = &\left\{\tilde{V}_H[\tilde{n}_{kl\tau} + \hat{n}_{kl\tau}] + \frac{\delta^2 E_{\mathrm{xc}}}{\delta n^{\sigma}\delta n^{\tau}}(\tilde{n}_{kl\tau} + \hat{n}_{kl\tau})\right\} \\ &|\tilde{\psi}_{j\sigma}\rangle + \sum_{IJ}|\tilde{p}_I\rangle\hat{D}_{IJ}\Bigg[\tilde{V}_H[\tilde{n}_{kl\tau} + \hat{n}_{kl\tau}] \\ &+ \frac{\delta^2 E_{\mathrm{xc}}}{\delta n^{\sigma}\delta n^{\tau}}(\tilde{n}_{kl\tau} + \hat{n}_{kl\tau})\Bigg]\langle\tilde{p}_J|\tilde{\psi}_{j\sigma}\rangle \\ &+ \sum_{IJ,I'J'}|\tilde{p}_I\rangle\langle\tilde{p}_J|\tilde{\psi}_{j\sigma}\rangle\frac{\delta^2(E^1 - \tilde{E}^1)}{\delta\rho^{\sigma}_{IJ}\delta\rho^{\tau}_{I'J'}}\langle\tilde{\psi}_{k\tau}|\tilde{p}_{I'}\rangle \\ &\langle\tilde{p}_{J'}|\tilde{\psi}_{l\tau}\rangle + \delta_{\sigma\tau}\langle\tilde{\psi}_{j\sigma}|\tilde{K}_{\mathrm{RSH}}|\tilde{\psi}_{k\sigma}\tilde{\psi}_{l\sigma}\rangle\end{aligned} \tag{27}$$

where $\tilde{V}_{\mathrm{H}}$ is the Hartree potential. The RSH part in the kernel functional is expressed by

$$\begin{aligned}\langle\tilde{\psi}_{j\sigma}|\tilde{K}_{\mathrm{RSH}}|\tilde{\psi}_{k\sigma}\tilde{\psi}_{l\sigma}\rangle = &-\tilde{V}_{\mathrm{RSH}}[\tilde{n}_{kj\sigma} + \hat{n}_{kj\sigma}]|\tilde{\psi}_{l\sigma}\rangle \\ &- \sum_{IJ}|\tilde{p}_I\rangle\hat{D}[\tilde{V}_{\mathrm{RSH}}]\langle\tilde{p}_J|\tilde{\psi}_{l\sigma}\rangle \\ &- \sum_{(I,K)(J,L)}(K^1_{IJLK} - \tilde{K}^1_{IJLK})|\tilde{p}_I\rangle\langle\tilde{p}_K|\tilde{\psi}_{j\sigma}\rangle \\ &\langle\tilde{\psi}_{k\sigma}|\tilde{p}_L\rangle\langle\tilde{p}_J|\tilde{\psi}_{l\sigma}\rangle\end{aligned} \tag{28}$$

The occupied-projected random orbital (eq 9) and random linear-response orbital (eq 16) in PAW are

$$|\tilde{\eta}_{\sigma}\rangle = \sum_{i}|\tilde{\psi}_{i\sigma}\rangle\langle\tilde{\psi}_{i\sigma}|\tilde{S}^{1/2}|\xi\rangle \tag{29}$$

and

$$|\tilde{\eta}^{\pm}_{\sigma}\rangle = \sum_{i}|\tilde{\psi}^{\pm}_{i\sigma}\rangle\langle\tilde{\psi}_{i\sigma}|\tilde{S}^{1/2}|\xi\rangle \tag{30}$$

respectively. The stochastic orbital $|\tilde{\chi}_{\sigma}\rangle$ (eq 14) and the stochastic linear-response orbital $|\tilde{\chi}^{\pm}_{\sigma}\rangle$ (eq 18) are then

$$|\tilde{\chi}_{\sigma}\rangle = \zeta(r)|\tilde{\eta}_{\sigma}\rangle + \sum_{IJLM}|\tilde{p}_I\rangle\langle\tilde{p}_J|\tilde{\eta}_{\sigma}\rangle\int\hat{Q}^{LM}_{IJ}(r')\zeta(r')\mathrm{d}r' \tag{31}$$

and

$$|\tilde{\chi}^{\pm}_{\sigma}\rangle = \zeta(r)|\tilde{\eta}^{\pm}_{\sigma}\rangle + \sum_{IJLM}|\tilde{p}_I\rangle\langle\tilde{p}_J|\tilde{\eta}^{\pm}_{\sigma}\rangle\int\hat{Q}^{LM}_{IJ}(r')\zeta(r')\mathrm{d}r' \tag{32}$$

The stochastic RSH (eq 15) is thus reformulated within PAW as

$$\begin{aligned}\tilde{k}^{\gamma}_{\sigma}|\tilde{\psi}_{i\sigma}\rangle = &-[|\tilde{\chi}_{\sigma}\rangle\langle\tilde{\chi}_{\sigma}|\tilde{\psi}_{i\sigma}\rangle]_{\xi,\varphi} - \sum_{(I,K)(J,L)}(K^1_{IJLK} - \tilde{K}^1_{IJLK})|\tilde{p}_I\rangle \\ &\langle\tilde{p}_K|\tilde{\psi}_{i\sigma}\rangle[\tilde{p}_J|\tilde{\eta}_{\sigma}\rangle\langle\tilde{\eta}_{\sigma}|\tilde{p}_L\rangle]_{\xi}\end{aligned} \tag{33}$$

Similarly, eqs 19 and 20 are re-expressed as

$$\begin{aligned}&\sum_{j}\langle\tilde{\psi}_{i\sigma}|\tilde{K}_{\mathrm{RSH}}|\tilde{\psi}_{j\sigma}\tilde{\psi}^{\pm}_{j\sigma}\rangle \\ &= -[|\tilde{\chi}^{\pm}_{\sigma}\rangle\langle\tilde{\chi}_{\sigma}|\tilde{\psi}_{i\sigma}\rangle]_{\xi,\varphi} - \sum_{(I,K)(J,L)}(K^1_{IJLK} - \tilde{K}^1_{IJLK})|\tilde{p}_I\rangle\langle\tilde{p}_K| \\ &\tilde{\psi}_{i\sigma}\rangle[\tilde{p}_J|\tilde{\eta}^{\pm}_{\sigma}\rangle\langle\tilde{\eta}_{\sigma}|\tilde{p}_L\rangle_{\xi}\end{aligned} \tag{34}$$

https://dx.doi.org/10.1021/acs.jctc.9b01121
J. Chem. Theory Comput. 2020, 16, 1064−1072

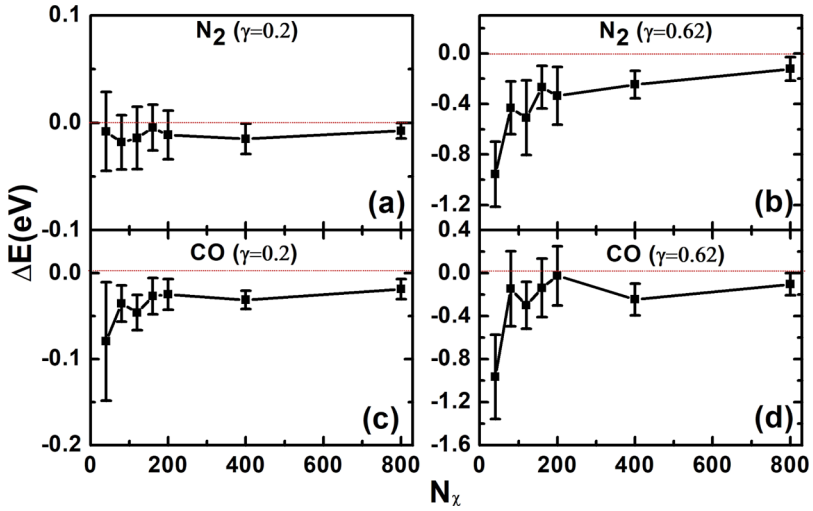

Figure 1. Energy difference between the stochastic and deterministic results of the lowest-energy singlet excited state as a function of the number of stochastic orbitals N_χ for the N_2 molecule with (a) $\gamma = 0.2$ Å^{-1} and (b) $\gamma = 0.62$ Å^{-1} and the CO molecule with (c) $\gamma = 0.2$ Å^{-1} and (d) $\gamma = 0.62$ Å^{-1}. The error bars scale the statistical errors. The red-dashed lines indicate the zero difference.

and

$$\sum_j \langle\tilde{\psi}_{i\sigma}|\tilde{K}_{\mathrm{RSH}}|\tilde{\psi}^{\pm}_{j\sigma}\tilde{\psi}_{j\sigma}\rangle = -[|\tilde{\chi}_\sigma\rangle\langle\tilde{\chi}^{\pm}_\sigma|\tilde{\psi}_{i\sigma}\rangle]_{\xi,\varphi} - \sum_{(I,K)(J,L)} (K^1_{IJLK} - \tilde{K}^1_{IJLK})|\tilde{p}_I\rangle\langle\tilde{p}_K| \tilde{\psi}_{i\sigma}\rangle[\tilde{p}_J|\tilde{\eta}_\sigma\rangle\langle\tilde{\eta}^{\pm}_\sigma|\tilde{p}_L\rangle_\xi \quad (35)$$

The ionic force in the excited state is obtained as the negative derivative of the Lagrangian $\hat{\mathcal{L}}_\alpha$ at its stationary point. Because $\hat{\mathcal{L}}_\alpha$ is fully variational, the first-order derivative with respect to an ionic coordinate x does not involve any chain-rule derivatives of its variables, that is, KS orbitals, linear-response orbitals, and stochastic orbitals. Thus, the partial derivatives of the RSH elements in $\hat{\mathcal{L}}_\alpha$ are entirely because of the explicit dependence of the PAW projector functions $|\tilde{p}_I\rangle$ and the function $\hat{Q}^{LM}_{IJ}$ on x. The partial derivatives of the stochastic RSH elements in the GKS Hamiltonian is

$$\left\langle\tilde{\psi}_{i\sigma}\left|\frac{\partial\tilde{k}^\gamma_\sigma}{\partial x}\right|\tilde{\psi}_{j\sigma}\right\rangle = -\left[\frac{\partial\langle\tilde{\psi}_{i\sigma}|\tilde{\chi}_\sigma\rangle}{\partial x}\langle\tilde{\chi}_\sigma|\tilde{\psi}_{j\sigma}\rangle + \langle\tilde{\psi}_{i\sigma}|\tilde{\chi}_\sigma\rangle\frac{\partial\langle\tilde{\chi}_\sigma|\tilde{\psi}_{j\sigma}\rangle}{\partial x}\right]_{\xi,\varphi} - \sum_{(I,K)(J,L)} K^1_{IJLK} - \tilde{K}^1_{IJLK} \left\{\frac{\partial\langle\tilde{\psi}_{i\sigma}|\tilde{p}_I\rangle\langle\tilde{p}_K|\tilde{\psi}_{j\sigma}\rangle}{\partial x}[\langle\tilde{p}_J|\tilde{\eta}_\sigma\rangle\langle\tilde{\eta}_\sigma|\tilde{p}_L\rangle]_\xi + \langle\tilde{\psi}_{i\sigma}|\tilde{p}_I\rangle\langle\tilde{p}_K|\tilde{\psi}_{j\sigma}\rangle\left[\frac{\partial\langle\tilde{p}_J|\tilde{\eta}_\sigma\rangle\langle\tilde{\eta}_\sigma|\tilde{p}_L\rangle}{\partial x}\right]_\xi\right\} \quad (36)$$

where the partial derivative of an inner product between a KS orbital and a stochastic orbital is calculated by

$$\frac{\partial\langle\tilde{\psi}_{i\sigma}|\tilde{\chi}_\sigma\rangle}{\partial x} = \sum_{IJLM}\frac{\partial\langle\tilde{\psi}_{i\sigma}|\tilde{p}_I\rangle\langle\tilde{p}_J|\tilde{\eta}_\sigma\rangle}{\partial x}\int\hat{Q}^{LM}_{IJ}(\vec{r}')\zeta(\vec{r}')\mathrm{d}\vec{r}' + \sum_{IJLM}\langle\tilde{\psi}_{i\sigma}|\tilde{p}_I\rangle\langle\tilde{p}_J|\tilde{\eta}_\sigma\rangle\int\frac{\partial\hat{Q}^{LM}_{IJ}(\vec{r}')}{\partial x}\zeta(\vec{r}')\mathrm{d}\vec{r}' \quad (37)$$

The partial derivative of stochastic RSH elements in the kernel functional is similarly calculated. For example,

$$\frac{\partial\sum_{ij\sigma}\langle\tilde{\psi}^{\pm}_{i\sigma}\tilde{\psi}_{i\sigma}|\tilde{K}_{\mathrm{RSH}}|\tilde{\psi}_{j\sigma}\tilde{\psi}^{\pm}_{j\sigma}\rangle}{\partial x} = -\sum_{i\sigma}\left[\frac{\partial\langle\tilde{\psi}^{\pm}_{i\sigma}|\tilde{\chi}^{\pm}_\sigma\rangle}{\partial x}\langle\tilde{\chi}_\sigma|\tilde{\psi}_{j\sigma}\rangle + \langle\tilde{\psi}^{\pm}_{i\sigma}|\tilde{\chi}^{\pm}_\sigma\rangle\frac{\partial\langle\tilde{\chi}_\sigma|\tilde{\psi}_{i\sigma}\rangle}{\partial x}\right]_{\xi,\varphi} - \sum_{i\sigma(I,K)(J,L)}(K^1_{IJLK} - \tilde{K}^1_{IJLK}) \left\{\frac{\partial\langle\tilde{\psi}^{\pm}_{i\sigma}|\tilde{p}_I\rangle\langle\tilde{p}_K|\tilde{\psi}_{i\sigma}\rangle}{\partial x}[\langle\tilde{p}_J|\tilde{\eta}^{\pm}_\sigma\rangle\langle\tilde{\eta}_\sigma|\tilde{p}_L\rangle]_\xi + \langle\tilde{\psi}^{\pm}_{i\sigma}|\tilde{p}_I\rangle\langle\tilde{p}_K|\tilde{\psi}_{i\sigma}\rangle\left[\frac{\partial\langle\tilde{p}_J|\tilde{\eta}^{\pm}_\sigma\rangle\langle\tilde{\eta}_\sigma|\tilde{p}_L\rangle}{\partial x}\right]_\xi\right\} \quad (38)$$

III. NUMERICAL EXAMPLES

The approach presented here is general and can be implemented in any plane-wave PAW software package as a plug-and-compute module. In the present work, the ground-state calculations are carried out with the Vienna Ab Initio Simulation Package (VASP).[59,60] To expedite the self-consistent convergence, the fully self-consistent ground-state GKS-DFT calculations are performed following a few non-self-consistent DFT iterations without the stochastic RSH potential. The ground-state charge density and KS orbitals are then taken as the input for GKS-TDDFT which is used to

https://dx.doi.org/10.1021/acs.jctc.9b01121
J. Chem. Theory Comput. 2020, 16, 1064−1072

compute the excited-state properties, including excitation energy, exciton charge density, and ionic force.

To validate the stochastic formulation, we calculate the excitation energy of the lowest-energy singlet excited state for two small molecules, N_2 and CO. The spin-restricted ground-state calculations are performed with supercell dimensions of 20 Å × 20 Å × 20 Å. The energy cutoff of the plane-wave basis is 400 eV. Here, the local adiabatic XC functional is the Perdew−Burke−Ernzerhof (PBE) GGA.[61] The short-range exchange interaction is incorporated by modifying the conventional GGA exchange.[46]

We use $\gamma = 0.62$ Å^{-1} for the range-separation parameter, a value that has been successfully used for these two molecules.[62] To examine the effect of γ on the statistical errors, we have also considered a smaller range-separation parameter $\gamma = 0.2$ Å^{-1}. Figure 1 depicts the energy difference between the stochastic and deterministic values of the excitation energy as a function of the number of stochastic orbitals N_χ. The expectation values are estimated from 10 samples of independent stochastic TDDFT simulations, each with a different set of random functions $|\xi\rangle$. The statistical errors are estimated from the standard deviation of these 10 samples. Clearly, the excitation energies converge as N_χ increases. In addition, the stochastic fluctuations become smaller as the range-separation parameter decreases. Thus, a smaller value of N_χ is sufficient for convergence when γ is smaller. For example, with $N_\chi = 40$, the energy fluctuation of N_2 is within 0.05 eV for $\gamma = 0.2$ Å^{-1}, while it is about 0.5 eV for $\gamma = 0.62$ Å^{-1}. Similarly, for the smaller γ, $N_\chi = 200$ converges the excitation energy with a statistical error less than 0.02 eV. However, for the larger γ, $N_\chi > 800$ is necessary for a statistical error of less than 0.1 eV.

Similar results have been observed previously in the calculation of the GKS-DFT orbital energy for hydrogen-passivated silicon nanocrystals.[40] The reduction of stochastic fluctuations is due to a smaller contribution of the nonlocal exchange to the one-body Hamiltonian for smaller γ. The fact that the number of stochastic orbitals decreases with the system size makes the current method very appealing for solids, where explicit exchange is needed only at long distances, that is, the range-separation parameter is usually much smaller than that in molecules.[63] Further, while the reduction in γ (and therefore the reduction in N_χ) was only studied here for excitonic states, we expect that an even smaller γ (and therefore a smaller N_χ) would be required for charge transfer excitations where the charge is more separated.

As shown in Figure 1, the convergence of the GKS-TDDFT energy is always from below, that is, at a finite N_χ, the results will have a slight bias toward smaller excitations. A finite N_χ simulation yields excitations that have a statistical deviation (decreasing by $1/\sqrt{N_\chi}$) around an average value which is slightly different from the infinite-N_χ limit (i.e., the deterministic) by an amount-labeled "bias". The bias decreases by $1/N_\chi$ and is a general phenomenon in stochastic simulations that involve self-consistency or more general iterations. Such bias appears, for example, in stochastic DFT[42,64] and GF2.[65]

Next, we apply the method to an extended system of 2D MoS_2. The pristine 2D MoS_2 is modeled by (9 × 9) units with 81 Mo atoms and 162 S atoms. There are 1458 valence electrons in this system. In the GKS-TDDFT calculations, 80 occupied orbitals are included. We confirmed that this number yields converged results for both energy and ionic force of the lowest-energy excited state. The GKS-TDDFT calculations are performed without the spin−orbit coupling. The optimal value of the range-separation parameter is found to be $\gamma = 0.07$ Å^{-1} for 2D MoS_2. $N_\chi = 80$ stochastic orbitals are sufficient for converging both the fundamental and optical band gaps with a statistical error of less than 0.01 eV. Furthermore, because of the small value of γ, the bias is tiny (less than 5 meV) and the statistical error is also tiny, less than 0.01 eV.

The fundamental band gap (E_g) is found to be 2.78 eV, and the optical band gap (E_{opt}) is found to be 1.71 eV. The exciton binding energy, defined as $E_b = E_g - E_{opt}$, is thus 1.07 eV. These values are in very good agreement with previous GW-BSE results ($E_g = 2.84$ eV, $E_{opt} = 1.88$ eV, and $E_b = 0.96$ eV)[66] and ($E_g = 2.82$ eV, $E_{opt} = 1.78$ eV, and $E_b = 1.04$ eV)[67] for the infinite 2D MoS_2 sheet. In Figure 2a, we show the charge

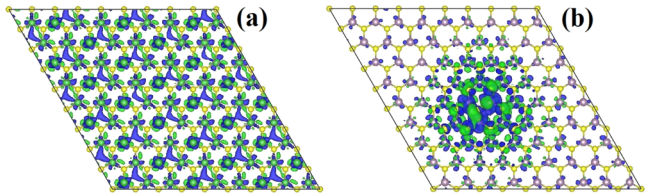

Figure 2. Charge densities of lowest-energy singlet excitons in (a) pristine MoS_2 and (b) MoS_2 with a single S vacancy. The charge density of the electron and the hole is colored green and blue, respectively. The isosurface levels are set at 9×10^{-5} e/Å^3 in (a) and 3×10^{-4} e/Å^3 in (b). The purple and yellow spheres represent Mo and S atoms, respectively.

density of the lowest-energy singlet exciton in pristine MoS_2. The electron (green) and hole (blue) projections are delocalized over the 2D plane, characteristic of a Mott−Wannier exciton. The Bohr radius of the exciton cannot be extracted from the exciton charge density. Instead, it can be estimated based on the two-particle wave function and this is left open for future study. We note that despite the underestimation of the fundamental band gap $E_g = 1.68$ eV and the neglection of excitonic binding, the PBE functional provides a good estimate of the optical band gap, $E_{opt} = 1.69$ eV, due to cancellation of errors.

We also examine a point defect in MoS_2, an S vacancy, which is abundant because of its low formation energy.[68] This vacancy is modeled by removing an S atom in the middle of the supercell. The local minimum of the ground state (m_0) and first excited state (m_1) potential energy surfaces are obtained through geometric relaxation using GKS-DFT and GKS-TDDFT, respectively, in the presence of the S vacancy. The force convergence criterion for geometric relaxation is 0.03 eV/Å.

We find that the exciton induces a local lattice distortion and is trapped around the S vacancy as manifested by the localized electron and hole, as shown in Figure 2b. This polaronic effect is quantitatively characterized by the polaronic binding energy, E_{pol}, the difference in the total energy (ground-state energy plus excitation energy) between the m_0 and m_1 geometries. The polaronic binding energy obtained using the stochastic RSH functional is $E_{pol} = 0.1$ eV. We also performed a geometric relaxation of the excited state with the PBE functional that yields a polaronic binding energy of $E_{pol} = 0.08$ eV, comparing very well with the RSH result. Thus, PBE could also provide reliable ionic forces of the excited state in addition to the good estimation of the excitation energy in the MoS_2 system.

https://dx.doi.org/10.1021/acs.jctc.9b01121
J. Chem. Theory Comput. 2020, 16, 1064−1072

The S vacancy induces two unoccupied defect levels within the gap, reducing the fundamental gap from E_g = 2.78 eV in pristine MoS_2 to E_g = 2.16 eV in the m_1 geometry. The optical gap is also decreased from E_g = 1.71 eV in pristine MoS_2 to E_g = 1.09 eV in m_1. Despite the significant difference in exciton charge density between the pristine and defective MoS_2, that is, delocalization versus localization in real space, the exciton binding energies of the two systems are the same, E_b = 1.07 eV. Therefore, the S vacancy does not affect the electron−hole interaction but could drastically influence their mobility in MoS_2. Previous GW-BSE calculations of $MoSe_2$ also found that the exciton binding energy remained essentially the same in the presence of the chalcogen vacancy.[69]

IV. CONCLUSIONS

In summary, we have reformulated plane-wave based GKS-TDDFT using a stochastic representation of the optimally tuned RSH functional. The computational cost associated with the exchange operator is significantly reduced by treating the zero-order and first-order KS density matrix with stochastic orbitals and a stochastic decomposition of the Coulomb convolution. For large systems, the method is almost as efficient as a local-potential KS-TDDFT.

Applications to small molecules, N_2 and CO, show that the statistical error induced by the stochastic formulation is controlled by increasing the number of stochastic orbitals and is significantly reduced by using a smaller range-separation parameter. This makes the current method very appealing for extended systems, as demonstrated here by simulating a 2D MoS_2 sheet with ∼1500 valence electrons. The fundamental gap, optical gap, and exciton binding energy of pristine MoS_2 obtained with an optimally tuned range-separation parameter compare very well with previous GW-BSE results. The fundamental gap and optical gap are reduced in the presence of S vacancy because of the defect-induced gap states, while the exciton binding energy is not changed. The S vacancy could trap the exciton where both the electron and hole are localized around the defect with a polaronic binding energy of 0.1 eV.

AUTHOR INFORMATION

Corresponding Authors

Xu Zhang − *California State University Northridge, Northridge, California;* orcid.org/0000-0002-6491-3234; Email: xu.zhang@csun.edu

Daniel Neuhauser − *University of California at Los Angeles, Los Angeles, California*; Email: dxn@ucla.edu

Other Authors

Gang Lu − *California State University Northridge, Northridge, California;* orcid.org/0000-0002-9168-8968

Roi Baer − *The Hebrew University of Jerusalem, Jerusalem, Israel;* orcid.org/0000-0001-8432-1925

Eran Rabani − *University of California, Berkeley, California, Lawrence Berkeley National Laboratory, Berkeley, California, and Tel Aviv University, Tel Aviv, Israel;* orcid.org/0000-0003-2031-3525

Complete contact information is available at: https://pubs.acs.org/10.1021/acs.jctc.9b01121

Notes

The authors declare no competing financial interest.

ACKNOWLEDGMENTS

X.Z. and G.L. acknowledge the support of the National Science Foundation (DMR-1828019 and DMR-1922042). E.R. acknowledges support from the Department of Energy, Photonics at Thermodynamic Limits Energy Frontier Research Center, under grant no. DE-SC0019140. D.N. acknowledges support from the National Science Foundation, CHE-1763176.

REFERENCES

(1) Runge, E.; Gross, E. K. U. Density-Functional Theory for Time-Dependent Systems. *Phys. Rev. Lett.* **1984**, *52*, 997.

(2) Marques, M. A. L.; Gross, E. K. U. Time-Dependent Density Functional Theory. *Annu. Rev. Phys. Chem.* **2004**, *55*, 427−455.

(3) Casida, M. E. *Recent Advances in Density Functional Methods*; D. P., Chong, Ed.; World Scientific: Singapore, 1995; pp 155−192.

(4) Petersilka, M.; Gossmann, U. J.; Gross, E. K. U. Excitation Energies from Time-Dependent Density-Functional Theory. *Phys. Rev. Lett.* **1996**, *76*, 1212.

(5) Bauernschmitt, R.; Ahlrichs, R. Treatment of Electronic Excitations within the Adiabatic Approximation of Time Dependent Density Functional Theory. *Chem. Phys. Lett.* **1996**, *256*, 454.

(6) Vasiliev, I.; Öğüt, S.; Chelikowsky, J. R. Ab Initio Excitation Spectra and Collective Electronic Response in Atoms and Clusters. *Phys. Rev. Lett.* **1999**, *82*, 1919.

(7) Walker, B.; Gebauer, R. Ultrasoft Pseudopotentials in Time-dependent Density-functional Theory. *J. Chem. Phys.* **2007**, *127*, 164106.

(8) van Caillie, C.; Amos, R. D. Geometric Derivatives of Excitation Energies using SCF and DFT. *Chem. Phys. Lett.* **2000**, *308*, 249.

(9) Furche, F.; Ahlrichs, R. Adiabatic Time-dependent Density Functional Methods for Excited State Properties. *J. Chem. Phys.* **2002**, *117*, 7433.

(10) Hutter, J. Excited State Nuclear Forces from the Tamm−Dancoff Approximation to Time-Dependent Density Functional Theory within the Plane Wave Basis Set Framework. *J. Chem. Phys.* **2003**, *118*, 3928.

(11) Zhang, X.; Lu, G. Subspace Formulation of Time-Dependent Density Functional Theory for Large-Scale Calculations. *J. Chem. Phys.* **2015**, *143*, 064110.

(12) Send, R.; Furche, F. First-order Nonadiabatic Couplings from Time-dependent Hybrid Density Functional Response Theory: Consistent Formalism, Implementation, and Performance. *J. Chem. Phys.* **2010**, *132*, 044107.

(13) Li, Z.; Suo, B.; Liu, W. First-order Nonadiabatic Coupling Matrix Elements Between Excited States: Implementation and Application at the TD-DFT and pp-TDA levels. *J. Chem. Phys.* **2014**, *141*, 244105.

(14) Ou, Q.; Bellchambers, G. D.; Furche, F.; Subotnik, J. E. First-order Derivative Couplings Between Excited States from adiabatic TDDFT Response Theory. *J. Chem. Phys.* **2015**, *142*, 064114.

(15) Zhang, X.; Lu, G. First-order Nonadiabatic Couplings in Extended Systems by Time-Dependent Density Functional Theory. *J. Chem. Phys.* **2018**, *149*, 244103.

(16) Gonze, X.; Ghosez, P.; Godby, R. W. Density-polarization Functional Theory of the Response of a Periodic Insulating Solid to an Electric Field. *Phys. Rev. Lett.* **1995**, *74*, 4035.

(17) Ghosez, P.; Gonze, X.; Godby, R. W. Long-wavelength Behavior of the Exchange-Correlation Kernel in the Kohn-Sham Theory of Periodic Systems. *Phys. Rev. B: Condens. Matter Mater. Phys.* **1997**, *56*, 12811.

(18) Kim, Y.-H.; Görling, A. Excitonic Optical Spectrum of Semiconductors Obtained by Time-dependent Density-functional Theory with the Exact-exchange Kernel. *Phys. Rev. Lett.* **2002**, *89*, 096402.

(19) Kümmel, S.; Kronik, L. Orbital-Dependent Density Functionals: Theory and Applications. *Rev. Mod. Phys.* **2008**, *80*, 3−60.
(20) Stein, T.; Eisenberg, H.; Kronik, L.; Baer, R. Fundamental Gaps in Finite Systems from Eigenvalues of a Generalized Kohn-Sham Method. *Phys. Rev. Lett.* **2010**, *105*, 266802.
(21) Seidl, A.; Görling, A.; Vogl, P.; Majewski, J. A.; Majewski, J. A.; Levy, M. Generalized Kohn-Sham Schemes and the Band-Gap Problem. *Phys. Rev. B: Condens. Matter Mater. Phys.* **1996**, *53*, 3764.
(22) Baer, R.; Neuhauser, D. A Density Functional Theory with Correct Long-Range Asymptotic Behavior. *Phys. Rev. Lett.* **2005**, *94*, 043002.
(23) Yang, Z.-h.; Sottile, F.; Ullrich, C. A. Simple Screened Exact-Exchange Approach for Excitonic Properties in Solids. *Phys. Rev. B: Condens. Matter Mater. Phys.* **2015**, *92*, 035202.
(24) Refaely-Abramson, S.; Jain, M.; Sharifzadeh, S.; Neaton, J. B.; Kronik, L. Solid-State Optical Absorption from Optimally Tuned Time-Dependent Range-Separated Hybrid Density Functional Theory. *Phys. Rev. B: Condens. Matter Mater. Phys.* **2015**, *92*, 081204.
(25) Kronik, L.; Neaton, J. B. Excited-State Properties of Molecular Solids from First Principles. *Annu. Rev. Phys. Chem.* **2016**, *67*, 587−616.
(26) Skone, J. H.; Govoni, M.; Galli, G. Nonempirical Range-Separated Hybrid Functionals for Solids and Molecules. *Phys. Rev. B* **2016**, *93*, 235106.
(27) Lopata, K.; Govind, N. Modeling Fast Electron Dynamics with Real-Time Time-Dependent Density Functional Theory: Application to Small Molecules and Chromophores. *J. Chem. Theory Comput.* **2011**, *7*, 1344−1355.
(28) Sissay, A.; Abanador, P.; Mauger, F.; Gaarde, M.; Schafer, K. J.; Lopata, K. Angle-Dependent Strong-field Molecular Ionization Rates with Tuned Range-separated Time-dependent Density Functional Theory. *J. Chem. Phys.* **2016**, *145*, 094105.
(29) Bruner, A.; Hernandez, S.; Mauger, F.; Abanador, P. M.; LaMaster, D. J.; Gaarde, M. B.; Schafer, K. J.; Lopata, K. Attosecond Charge Migration with TDDFT: Accurate Dynamics from a Well-Defined Initial State. *J. Phys. Chem. Lett.* **2017**, *8*, 3991−3996.
(30) Furche, F.; Burke, K. Time-Dependent Density Functional Theoryin Quantum Chemistry. *Annu. Rep. Comput. Chem.* **2005**, *1*, 19.
(31) Casida, M. E.; Huix-Rotllant, M. Progress in Time-Dependent Density-Functional Theory. *Annu. Rev. Phys. Chem.* **2012**, *63*, 287−323.
(32) Friesner, R. A. Ab Initio Quantum Chemistry: Methodology and Applications. *Proc. Natl. Acad. Sci. U.S.A.* **2005**, *102*, 6648−6653.
(33) Marzari, N.; Vanderbilt, D. Maximally Localized Generalized Wannier Functions for Composite Energy Bands. *Phys. Rev. B: Condens. Matter Mater. Phys.* **1997**, *56*, 12847.
(34) Marzari, N.; Mostofi, A. A.; Yates, J. R.; Souza, I.; Vanderbilt, D. Maximally Localized Wannier Functions: Theory and Applications. *Rev. Mod. Phys.* **2012**, *84*, 1419.
(35) Gygi, G. Compact Representations of Kohn-Sham Invariant Subspaces. *Phys. Rev. Lett.* **2009**, *102*, 166406.
(36) Wu, X.; Selloni, A.; Car, R. Order-N Implementation of Exact Exchange in Extended Insulating Systems. *Phys. Rev. B: Condens. Matter Mater. Phys.* **2009**, *79*, 085102.
(37) Gygi, F.; Duchemin, I. Efficient Computation of Hartree−Fock Exchange Using Recursive Subspace Bisection. *J. Chem. Theory Comput.* **2013**, *9*, 582−587.
(38) Damle, A.; Lin, L.; Ying, L. Compressed Representation of Kohn−Sham Orbitals via Selected Columns of the Density Matrix. *J. Chem. Theory Comput.* **2015**, *11*, 1463.
(39) Lin, L. Adaptively Compressed Exchange Operator. *J. Chem. Theory Comput.* **2016**, *12*, 2242.
(40) Neuhauser, D.; Rabani, E.; Cytter, Y.; Baer, R. Stochastic Optimally Tuned Range-Separated Hybrid Density Functional Theory. *J. Phys. Chem. A* **2016**, *120*, 3071−3078.
(41) Vlček, V.; Baer, R.; Neuhauser, D. Stochastic Time-dependent DFT with Optimally Tuned Range-separated Hybrids: Application to Excitonic Effects in Large Phosphorene Sheets. *J. Chem. Phys.* **2019**, *150*, 184118.
(42) Baer, R.; Neuhauser, D.; Rabani, E. Self-Averaging Stochastic Kohn-Sham Density-Functional Theory. *Phys. Rev. Lett.* **2013**, *111*, 106402.
(43) Neuhauser, D.; Gao, Y.; Arntsen, C.; Karshenas, C.; Rabani, E.; Baer, R. Breaking the Theoretical Scaling Limit for Predicting Quasiparticle Energies: The Stochastic GW Approach. *Phys. Rev. Lett.* **2014**, *113*, 076402.
(44) Rabani, E.; Baer, R.; Neuhauser, D. Time-dependent Stochastic Bethe-Salpeter Approach. *Phys. Rev. B: Condens. Matter Mater. Phys.* **2015**, *91*, 235302.
(45) Savin, A.; Flad, H.-J. Density Functionals for the Yukawa Electron-Electron Interaction. *Int. J. Quantum Chem.* **1995**, *56*, 327.
(46) Iikura, H.; Tsuneda, T.; Yanai, T.; Hirao, K. A Long-range Correction Scheme for Generalized-Gradient-Approximation Exchange Functionals. *J. Chem. Phys.* **2001**, *115*, 3540.
(47) Yanai, T.; Tew, D. P.; Handy, N. C. A New Hybrid Exchange−Correlation Functional Using the Coulomb-attenuating Method (CAM-B3LYP). *Chem. Phys. Lett.* **2004**, *393*, 51.
(48) Vydrov, O. A.; Scuseria, G. E. Assessment of a Long-range Corrected Hybrid Functional. *J. Chem. Phys.* **2006**, *125*, 234109.
(49) Chai, J.-D.; Head-Gordon, M. Long-range Corrected Hybrid Density Functionals with Damped Atom−Atom Dispersion Corrections. *Phys. Chem. Chem. Phys.* **2008**, *10*, 6615.
(50) Blöchl, P. E. Projector augmented-wave method. *Phys. Rev. B: Condens. Matter Mater. Phys.* **1994**, *50*, 17953.
(51) Kresse, G.; Joubert, D. From Ultrasoft Pseudopotentials to the Projector Augmented-wave Method. *Phys. Rev. B: Condens. Matter Mater. Phys.* **1999**, *59*, 1758.
(52) Baer, R.; Neuhauser, D. Real-time Linear Response for Time-dependent Density-functional Theory. *J. Chem. Phys.* **2004**, *121*, 9803.
(53) Neuhauser, D.; Baer, R. Efficient Linear-response Method Circumventing the Exchange-Correlation Kernel: Theory for Molecular Conductance Under Finite Bias. *J. Chem. Phys.* **2005**, *123*, 204105.
(54) Stratmann, R. E.; Scuseria, G. E.; Frisch, M. J. An Efficient Implementation of Time-dependent Density-functional Theory for the Calculation of Excitation Energies of Large Molecules. *J. Chem. Phys.* **1998**, *109*, 8218.
(55) Hutchinson, M. F. A Stochastic Estimator of the Trace of the Influence Matrix for Laplacian Smoothing Splines. *Commun. Stat. Simulat. Comput.* **1990**, *19*, 433−450.
(56) Hamann, D. R.; Schlüter, M.; Chiang, C. Norm-Conserving Pseudopotentials. *Phys. Rev. Lett.* **1979**, *43*, 1494.
(57) Bachelet, G. B.; Hamann, D. R.; Schlüter, M. Pseudopotentials that Work: From H to Pu. *Phys. Rev. B: Condens. Matter Mater. Phys.* **1982**, *26*, 4199.
(58) Paier, J.; Hirschl, R.; Marsman, M.; Kresse, G. The Perdew−Burke−Ernzerhof Exchange-correlation Functional Applied to the G2-1 Test Set Using a Plane-wave Basis Set. *J. Chem. Phys.* **2005**, *122*, 234102.
(59) Kresse, G.; Hafner, J. Ab Initio Molecular Dynamics for Liquid Metals. *Phys. Rev. B: Condens. Matter Mater. Phys.* **1993**, *47*, 558.
(60) Kresse, G.; Furthmüller, J. Efficient Iterative Schemes for Ab Initio Total-Energy Calculations Using a Plane-Wave Basis Set. *Phys. Rev. B: Condens. Matter Mater. Phys.* **1996**, *54*, 11169.
(61) Perdew, J. P.; Burke, K.; Ernzerhof, M. Generalized Gradient Approximation Made Simple. *Phys. Rev. Lett.* **1996**, *77*, 3865.
(62) Tawada, Y.; Tsuneda, T.; Yanagisawa, S.; Yanai, T.; Hirao, K. A Long-range-corrected Time-dependent Density Functional Theory. *J. Chem. Phys.* **2004**, *120*, 8425.
(63) Eisenberg, H. R.; Baer, R. A New Generalized Kohn−Sham Method for Fundamental Band-Gaps in Solids. *Phys. Chem. Chem. Phys.* **2009**, *11*, 4674.
(64) Fabian, M. D.; Shpiro, B.; Rabani, E.; Neuhauser, D.; Baer, R. Stochastic Density Functional Theory. *Wiley Interdiscip. Rev.: Comput. Mol. Sci.* **2019**, *9*, No. e1412.

https://dx.doi.org/10.1021/acs.jctc.9b01121
J. Chem. Theory Comput. 2020, 16, 1064−1072

(65) Neuhauser, D.; Baer, R.; Zgid, D. Stochastic Self-Consistent Second-Order Green's Function Method for Correlation Energies of Large Electronic Systems. *J. Chem. Theory Comput.* **2017**, *13*, 5396.
(66) Qiu, D. Y.; da Jornada, F. H.; Louie, S. G. Optical Spectrum of MoS_2: Many-body Effects and Diversity of Exciton States. *Phys. Rev. Lett.* **2013**, *111*, 216805.
(67) Ramasubramaniam, A. Large Excitonic Effects in Monolayers of Molybdenum and Tungsten Dichalcogenides. *Phys. Rev. B: Condens. Matter Mater. Phys.* **2012**, *86*, 115409.
(68) Liu, D.; Guo, Y.; Fang, L.; Robertson, J. Sulfur Vacancies in Monolayer MoS_2 and Its Electrical Contacts. *Appl. Phys. Lett.* **2013**, *103*, 183113.
(69) Refaely-Abramson, S.; Qiu, D. Y.; Louie, S. G.; Neaton, J. B. Defect-Induced Modification of Low-Lying Excitons and Valley Selectivity in Monolayer Transition Metal Dichalcogenides. *Phys. Rev. Lett.* **2018**, *121*, 167402.

https://dx.doi.org/10.1021/acs.jctc.9b01121
J. Chem. Theory Comput. 2020, 16, 1064−1072